

BAYESIAN DATA FUSION APPROACHES TO PREDICTING SPATIAL TRACKS: APPLICATION TO MARINE MAMMALS

BY YANG LIU¹, JAMES V. ZIDEK¹, ANDREW W. TRITES
AND BRIAN C. BATTAILE

University of British Columbia

Bayesian Melding (BM) and downscaling are two Bayesian approaches commonly used to combine data from different sources for statistical inference. We extend these two approaches to combine accurate but sparse direct observations with another set of high-resolution but biased calculated observations. We use our methods to estimate the path of a moving or evolving object and apply them in a case study of tracking northern fur seals. To make the BM approach computationally feasible for high-dimensional (big) data, we exploit the properties of the processes along with approximations to the likelihood to break the high-dimensional problem into a series of lower dimensional problems. To implement the alternative, downscaling approach, we use R-INLA to connect the two sources of observations via a linear mixed effect model. We compare the predictions of the two approaches by cross-validation as well as simulations. Our results show that both approaches yield similar results—both provide accurate, high resolution estimates of the at-sea locations of the northern fur seals, as well as Bayesian credible intervals to characterize the uncertainty about the estimated movement paths.

1. Introduction. Recent technological advances have made it feasible to track many things, such as the foraging trips of endangered animals [Wilson et al. (2007)], the movements of basketball players Miller et al. (2014) and the spread of infectious diseases [Ginsberg et al. (2009), Lazer et al. (2014a)]. Foraging trips, for example, reflect the feeding areas of animals, and can be used to identify critical habitat. Similarly, the movements of basketball players can be summarized to identify playing strategies, and set up offensive and defensive plays [Liu et al. (2016a)]. Tracking of disease is essential for controlling epidemics and predicting future outbreaks. Tracking such things helps to understand the processes that determine movement patterns, and provides a means to forecast and plan for future changes.

Data collection technologies used for tracking involve both observations from both direct and indirect sources. Direct observations are usually accurate but sparse in space and time, such as GPS observations of an animal's location in animal

Received January 2016; revised May 2016.

¹Supported in part by the Natural Science and Engineering Research Council of Canada.

Key words and phrases. Bayesian melding, downscaling, bio-logging, conditional independence, INLA, Dead-Reckoning, tracking, marine mammals, Northern fur seal.

tracking or the number of infected patients from epidemic reports. In contrast, indirect sources are usually inaccurate but data rich, and can help to fill in the gaps in the direct observations, such as inferred locations between GPS observations (i.e., Dead-Reckoned paths) or the search fraction of flu related queries on Google [Ginsberg et al. (2009)]. Combining different systems of observations can ultimately result in more accurate and higher resolution tracks for objects of interest.

The problem of combining disparate data sets is not new to statisticians. In environmental statistics, for example, various approaches have been developed to combine measurements with numerical (computer) model outputs. Two of the most common approaches are Bayesian Melding (BM) [Fuentes and Raftery (2005)] and downscaling [Berrocal, Gelfand and Holland (2010), Zidek, Le and Liu (2012)]. Bayesian Melding was developed to combine direct observations of air-pollutant concentrations from a sparse network of monitoring stations with outputs by grid cell from a deterministic chemical transportation (computer) model in a geographical domain based on known pollutant source and geophysical information. In this approach, the direct observations and the computer model outputs are connected via a hidden process of the “true” air pollution level, that is, the monitoring stations’ observations $Z_0(s)$ at location s measure the true air pollutant level $Z(s)$ with some measurement error

$$Z_0(s) = Z(s) + e(s),$$

where $e(s) \stackrel{\text{i.i.d.}}{\sim} N(0, \sigma_e^2)$ is a white noise process independent of $Z(s)$. The computer model outputs $Z_1(t)$ are assumed to be

$$Z_1(s) = a(s) + b(s)Z(s) + \delta(s),$$

where $a(s)$ is the systematic additive error, $b(s)$ is the multiplicative error and $\delta(s)$ is the additional noise. Usually, the multiplicative error $b(s)$ is assumed to be a constant, and the additive error $a(s)$ is modeled with a polynomial or a Gaussian process with exponential covariance function [Foley and Fuentes (2008), Fuentes and Raftery (2005), Sahu, Gelfand and Holland (2010)]. The BM approach has been adapted for other uses, such as to model hurricane surface winds [Foley and Fuentes (2008)], ozone levels [Liu, Le and Zidek (2011)] and wet deposition [Sahu, Gelfand and Holland (2010)], etc. These applications have demonstrated the remarkable flexibility and effectiveness of the BM approach.

Despite its flexibility, the BM approach is computationally cumbersome when dealing with “change-of-support” problems [Berrocal, Gelfand and Holland (2010), Zidek, Le and Liu (2012)]—namely, where the observations are collected on different spatial scales, such as in situ station measurements versus area averages. In response, Berrocal, Gelfand and Holland (2010) developed a spatial or spatial-temporal downscaling approach to combine the air pollutant data using a linear mixed effect model. This downscaling approach can be described, using the

same notation as above, by the following regression model with spatially correlated coefficients:

$$Z_0(s) = \beta_0 + r_1(s) + (\beta_1 + r_2(s))Z_1(s) + \varepsilon(s),$$

where $r_1(s)$ and $r_2(s)$ are some spatial-temporal random processes, such as the Matérn process. Recently, Rundel et al. (2015) further developed the downscaling approach to combine speciated PM_{2.5} (particulate matter with a diameter of 2.5 micro-meters or less) levels from multiple monitoring networks and computer model outputs.

In this paper, we adapt both the BM and downscaling approaches to combine multiple sources of observations for tracking objects. We use both approaches to combine the GPS locations and Dead-Reckoned paths of marine mammals and apply them to data from northern fur seals—a species that inhabits the North Pacific Ocean [Battaile et al. (2015)]. Unlike combining the observation from monitoring networks and computer model outputs, we are less concerned with the spatial “change-of-support” problem in tracking, as the observations and model outputs in our application lie on the same time scale.

In the BM framework, we first choose a random process that reflects the nature of the tracked object or the physics of its evolution as the prior for $Z(t)$. For example, we consider $Z(t)$ as a Brownian Bridge process in our application to northern fur seal tracking, which corresponds to the fact that they return to their breeding beaches to feed their young after a foraging trip. To track an infectious disease, we could model $Z(t)$ with the susceptible–exposed–infected–recovered (SEIR) compartmental equation [Dukic, Lopes and Polson (2012)]. All the systems of observations are linked to different transformations of $Z(t)$: the direct observation $Z_0(t)$ is $Z(t)$ plus a white noise term, while the indirect observation $Z_1(t), Z_2(t), \dots$, are functions of $Z(t)$ plus some other random processes as biases that reflect model error. Our BM framework can be summarized as follows:

$$\begin{aligned}
 & Z(t) \sim \text{A certain random process,} \\
 & Z_0(t) = Z(t) + \varepsilon_0(t), \\
 (1.1) \quad & Z_1(t) = g_1(Z(t)) + \xi_1(t), \\
 & Z_2(t) = g_2(Z(t)) + \xi_2(t), \\
 & \dots \dots ,
 \end{aligned}$$

where $\varepsilon_0(t)$ is a white noise process, $g_j(\cdot), j = 1, 2, \dots$ is a function of $Z(t)$ and $\xi_j(t)$ is another random process. To make inference about $Z(t)$, we need to calculate the posterior distribution of $Z(t)|Z_0(t), Z_1(t), Z_2(t), \dots$, whose posterior mean can be the smoothed/predicted “track” of the tracking object and the posterior credible intervals (CI) reflect the uncertainty in the track. Note that the random process in (1.1), such as the Brownian Bridge or the SEIR process, only reflects our prior knowledge of the track. Its posterior is updated via the observations.

The downscaling approach for tracking bypasses the modeling of $Z(t)$ and builds the mixed effects model between the direct observations and the other systems of observation as

$$Z_0(t) = \beta_0 + r_0(t) + (\beta_1 + r_1(t))Z_1(t) + (\beta_2 + r_2(t))Z_2(t) + \cdots + \varepsilon(t),$$

where $r_j(t)$, $j = 0, 1, 2, \dots$ can be some Gaussian processes as in [Berrocal, Gelfand and Holland \(2010\)](#) and [Zidek, Le and Liu \(2012\)](#). As with the BM approach, the posterior mean and CI of the linear predictor can be the predicted “track” and its uncertainty.

For the tracking application, we need to first choose appropriate processes for the random components, such as $Z(t)$, $\xi_j(t)$, etc. Besides matching the physics of the tracked objects, we also need to take account of the computational burden. For example, devices attached to a northern fur seal (which samples at 16 Hz) and the video tracking of NBA players (which samples at 25 Hz) [[Liu et al. \(2016a\)](#)] both yield incredibly big data sets. As a result, we avoid using MCMC techniques that have been used in the past for both the BM and downscaling approaches. Instead, we fit the downscaling model with the integrated nested Laplace approximation (INLA) method developed in [Lindgren, Rue and Lindström \(2011\)](#) and [Rue, Martino and Chopin \(2009\)](#). Inspired by the sparse matrix techniques, likelihood approximations, and gradient based numeric integrations in the INLA approach, we exploit the properties of the processes and designed approximations to the likelihood for the BM approach.

The following describes the BM and downscaling approaches for tracking, and applies them to a case study of northern fur seals. We provide the background of this application in Section 2 with specific explanations of the two sources of observations. Section 3 describes our Bayesian Melding approach, while Section 4 describes the downscaling approach. We perform several simulation studies to evaluate our BM and downscaling approaches, which are reported in Section 5. Section 6 contains the case study results together with cross-validation comparisons. The conclusion and discussion are contained in Section 7.

2. Background and data. Marine biologists have been attaching a variety of different electronic tags to marine animals to track their movements, describe their behaviors and characterize their habitat preferences [e.g., [Benoit-Bird et al. \(2013a\)](#)]. Interactions of tracked animals with other animals or the environment allow for ecological questions regarding population structure and dynamics to be addressed [[Benoit-Bird et al. \(2013b\)](#), [Block et al. \(2011\)](#)]. Free-ranging animals can serve as sensors to collect environmental (e.g., oceanographic) data, which is difficult or expensive to obtain via conventional means such as ships or satellites [[Boehme, Kovacs and Lydersen \(2010\)](#), [Boehme et al. \(2008\)](#), [Nordstrom et al. \(2013\)](#)]. These environmental data can help to better understand ecosystems and the impact of climate change.

Accurately determining the locations of animals is a fundamental problem in animal tracking. One means of obtaining locations is to have tags carried by animals communicate with satellite systems such as the Global Positioning System (GPS) or the ARGOS satellites. Unfortunately, GPS tags have a limited sampling frequency due to a limited battery life, and often have limited exposure to satellites due to animal behavior and habitat. This is particularly true for marine mammals that dive frequently and are only on the surface for a relatively small proportion of time. Thus, satellite systems can only provide a sparse and irregularly spaced record of animal locations.

Many statistical methods have been developed to interpolate the GPS and ARGOS observations, and to filter outliers (especially in the ARGOS data). [McClintock et al. \(2014\)](#) provide an extensive review of this literature. Most of the approaches developed are state-space-based models either in continuous or discrete time and space, such as the continuous time correlated random walk (CRAWL) [[Johnson et al. \(2008\)](#)] or robust state-space models [[Jonsen, Flemming and Myers \(2005\)](#)]. Recently, [Fleming et al. \(2016\)](#) proposed Kriging to interpolate the satellite observations and compared the performance of several Gaussian processes with different covariance structures. However, these methods cannot deal with the Dead-Reckoned (DR) path as additional observations.

One means of collecting data on the animal's movements between observations from a GPS tag is to concurrently deploy a "Dead-Reckoning" (DR) tag consisting of an accelerometer, a magnetometer, a time-depth-recorder (TDR) and other supporting components [[Nordstrom et al. \(2013\)](#), [Wilson et al. \(2007\)](#)]. Such DR tags can sample at infra-second frequencies (e.g., 16 Hz) and provide a detailed record of an animal's movements. Data downloaded from the tag can be processed by a Dead-Reckoning algorithm (DRA) to reconstruct the Dead-Reckoned (DR) path of the animal [[Johnson and Tyack \(2003\)](#), [Wilson and Wilson \(1988\)](#), [Wilson et al. \(2007\)](#)].

The detailed implementation of a DRA may vary in different applications [[Elkaim et al. \(2006\)](#), [Wilson and Wilson \(1988\)](#), [Wilson et al. \(2007\)](#)], but the basic idea is as follows. First, the animal's orientation (direction of velocity) is estimated from the smoothed accelerometer and magnetometer readings via an approximate solution to Wahba's problem [[Wahba \(1965\)](#)]. Next, the animal's speed can be estimated by data from other sensors, such as a TDR or speed sensor [[Mitani et al. \(2003\)](#)]; or derived from acceleration data; or assumed to be a constant value. Speed is in turn combined with the orientation and a known starting point to create the DR path. A more detailed description of the DRA can be found in the supplementary material [[Liu et al. \(2016b\)](#)].

The DR path provides remarkably detailed information about an animal's movements, especially fine-scale fluctuations that the GPS cannot capture. However, the DR path can be biased because of poor measurements of swim speeds, systematic as well as random error in the accelerometer and magnetometer sensors, undocumented animal movements caused by ocean currents, confounding between

movement and gravitational acceleration, and discretization in the integration of the speed. All of these factors lead to biases and errors in the DR path [Liu et al. (2015), Wilson et al. (2007)], which can be significant if not corrected using the relatively accurate GPS observations (by as much as 100 km at the end of a seven-day trip in the case study we explored below).

The conventional approach to correct for DR path bias has been to add a linear bias correction term to the DR path, which directly shifts the DR path to the locations indicated by the GPS observations [Wilson et al. (2007)]. This approach can be summarized as follows: denote the DR path (in one dimension) by x_1, x_2, \dots, x_T at times $t = 1, 2, \dots, T$ and the GPS observations at times 1 and T by y_1, y_T , respectively; assume, without loss of generality, that $x_1 = y_1 = 0$ and that the corrected path $\hat{\eta}_t$ is calculated as

$$(2.1) \quad \hat{\eta}_t = x_t + \frac{y_T - x_T}{T - 1}(t - 1),$$

which evenly distributes the bias $y_T - x_T$ over the individual time points. The DR path between two GPS observations is shifted directly to the locations indicated by the GPS observations, namely, $\hat{\eta}_1 = y_1$ and $\hat{\eta}_T = y_T$. This procedure is repeated for all the sections separated by the GPS observations to correct the whole path.

Unfortunately, this conventional method to correct for the DR path bias is simplistic, and fails to consider the measurement error in the GPS observations. This conventional method also fails to provide a statement about the uncertainty in the corrected path. As a result, the biologging community has concerns about the validity of the corrected path [Battaile et al. (2015), Wilson et al. (2007)] and has generally been reluctant to assign too much significance to reconstructed locations. It is these concerns that prompted us to develop the Bayesian Melding and downscaling approaches as competing statistically rigorous methods for track reconstruction that overcomes the limitations of the conventional approach. We thus sought to correct the biased DR paths and quantify the uncertainty in the corrected paths.

The application in this paper involves tracking data from two lactating northern fur seals captured and tagged on Bogoslof Island (Alaska, USA) as part of the Bering Sea Integrated Research Program (BSIERP) [Benoit-Bird et al. (2013a), Nordstrom et al. (2013)]. Two tags were glued to the fur of each seal with five minute epoxy: a DR “Daily Diary” tag and a TDR MK 10-F with Fastloc®GPS technology (both manufactured by Wildlife Computers). The accelerometers and magnetometers of the DR tag were set to sample 16 times per second (16 Hz), while the TDR pressure sensor sampled at 1 Hz. The GPS sensor was programmed to make one attempt every 15 minutes to connect with the satellite.

We produced the DR path for two foraging trips made by the two female seals (denoted as “Trip 1” and “Trip 2”) using the “TrackReconstruction” R package on the 16 Hz data set. This R package was developed based on Wilson and Wilson (1988), Wilson et al. (2007) and described in detail by Battaile (2014). We later

TABLE 1

The sample quantiles in minutes of the time gaps between two consecutive GPS observations in our data

	Min	10%	25%	50%	75%	90%	Max
Trip 1	14.75	15.00	15.45	18.40	31.68	82.79	953.65
Trip 2	14.75	15.00	15.05	30.00	113.05	130.77	698.47

subsampled the DR path to various frequencies to fit the computational capacity of methods used to get the results. We also projected the GPS observations as longitude and latitude to Easting and Northing in kilometers (km) in a point-wise fashion as per [Wilson et al. \(2007\)](#).

The two foraging trips made by the fur seals in our study were each about 1 week in duration. Trip 1 was 7 days and had 274 valid GPS observations, while Trip 2 lasted about 7.5 days and had 130 GPS observations. A large proportion of the GPS locations had time gaps around 15 minutes (Table 1)—the designed time gap for the GPS device to record the locations. However, non-negligible proportions of them (13% in Trip 1 and 30% in Trip 2) were greater than 1 hour, and the longest time gap in both trips was longer than 10 hours. Thus, the GPS observations were irregularly spaced in time and space, and the duration of the gaps between them were quite large, making it necessary to incorporate the high resolution DR path. More detailed exploratory analysis of these data sets can be found in [Liu et al. \(2015\)](#).

3. Bayesian melding. In this section, we introduce the BM approach to combine the information from the accurate but sparse GPS observations with the biased but dense DR path. For simplicity, the two dimensions of the path (latitude and longitude) are dealt with separately. Abstractly, our theory is about a one-dimensional path over time, which we denote by $\eta(t)$ at discrete time points $t = 1, 2, \dots, T$. The time unit plays no essential role in our theory. The approach works just as well with unequally spaced time points, that is, for arbitrary t_1, t_2, \dots, t_T . But for expository simplicity we work with $1 : T$ because the DR paths are equally spaced. As in the previous BM literature, we put a Gaussian process prior on $\eta(t)$,

$$(3.1) \quad \boldsymbol{\eta}(1 : T) \sim N(\mathbf{f}(1 : T), \mathbf{R}(1 : T, 1 : T)),$$

where the $\mathbf{f}(\cdot)$ denotes the process mean function and \mathbf{R} its covariance matrix. The notation $\mathbf{f}(1 : T)$ stands for the vector $(f(1), f(2), \dots, f(T))^T$, while $\mathbf{R}(1 : T, 1 : T)$ is a $T \times T$ covariance matrix with $R(t, t') = \text{Cov}(\eta(t), \eta(t'))$. Throughout this paper, bold-faced characters are used exclusively to represent vectors or matrices.

Various options are available for this Gaussian process. A common one [[Fuentes and Raftery \(2005\)](#), [Sacks et al. \(1989\)](#)] assumes that \mathbf{f} is a simple parametric model, for example, a constant or a linear function of the covariates, and $R(t, t') =$

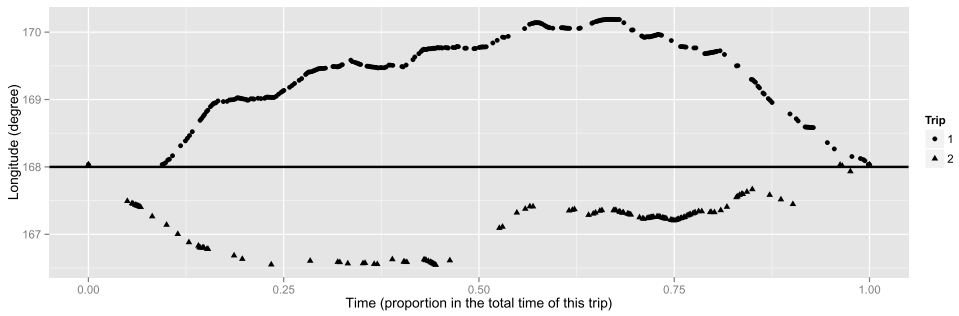


FIG. 1. The (negative) longitude of the GPS observations of the foraging trips made by two northern fur seals in our case study. Both trips started and ended at Bogoslof Island (Alaska) where the females gave birth and nursed their pups, and the horizontal line indicates the longitude $-168.035E$ of the island. The time unit is the proportion of the total time of this foraging trip. Notice the “bridge” structure of these trips (i.e., differences are small at the beginning and end, but very large in the middle). This “bridge” structure is described by the Brownian Bridge process.

$\sigma^2\rho(|t - t'|)$, where $\rho(\cdot)$ is an isotropic correlation function from a class such as the Matérn or power exponential. However, this popular stationary Gaussian process is not suitable for our application. As noted above, the tracked animal must return to the location from where it started its foraging trip (to reunite with her pup), which means that the start and end points of the track are fixed, as shown in Figure 1. Apart from the start and end points, the animal’s path is unknown, and hence random in our Bayesian framework. Its variation is relatively large in the middle and small when close to the known start and end points. These features of the path led us to model it with a Brownian Bridge process, whose mean and covariance functions are as follows:

$$f(t) = A + (B - A)\frac{t - 1}{T - 1},$$

$$R(s, t) = \sigma_H^2 \frac{(\min(s, t) - 1)(T - \max(s, t))}{(T - 1)},$$

where $\eta(1) = A$ and $\eta(T) = B$ are the known start and end points of the path, while σ_H^2 is the variance parameter. Notice that $R(1, \cdot) = R(\cdot, T) = 0$, in accordance with the known start and end points $\eta(1)$ and $\eta(T)$. Also, $R(t, t)$ increases with t when $t < (T - 1)/2$ and decreases with t for $t > (T - 1)/2$, reflecting the fact that the variation of the path is large in the middle. Another noteworthy property of our covariance matrix \mathbf{R} is its form as the product of a scalar σ^2 and a matrix, the latter depending only on the time points. To clearly represent the parameters of the Brownian Bridge process, we introduce the notation

$$(3.2) \quad \text{BB}(A, B, T_S, T_E, \sigma^2)$$

for a Brownian Bridge process, which starts from A at time T_S and ends in B at time T_E with a variance parameter σ^2 , namely, $f(t) = A + (B - A)(t - T_S)/(T_E -$

T_S) and covariance function $R(s, t) = \sigma_H^2(\min(s, t) - T_S)(T_E - \max(s, t))/((T_E - T_S))$.

Our choice of the Brownian Bridge prior is popular in the literature of biology and ecology. According to Humphries et al. (2010), marine mammals tend to exhibit Brownian-like movements in environments with abundant food resources, such as the resource-filled ocean around Bogoslof island where our case study was centered [Benoit-Bird et al. (2013b)]. Also, a Brownian Bridge model was proposed by Horne et al. (2007) to model the habitat usage of a wide range of animal species. This model was further improved by Kranstauber, Safi and Bartumeus (2014), Kranstauber et al. (2012) and Sawyer et al. (2009). Pozdnyakov et al. (2014) studied different ways of estimating the parameters of the Brownian Bridge model. Many other examples where an animal’s path has been modeled with Brownian Bridge processes can be found in the references of the above papers.

It should be recognized that the Brownian Bridge prior does not mean that the animal’s path after being updated with the GPS observations and the DR path is still a Brownian Bridge. We use the Brownian Bridge prior to motivate a proper covariance structure, whereby the beginning and end of the animal’s path are known but there is more uncertainty about the middle part of this path. The Markovian structure of the Brownian Bridge also helps to simplify the Bayesian computation of combining this process with the DR path, as discussed later.

The GPS observations of the locations are denoted by $Y(t_k), k = 1, 2, \dots, K, t_1 = 1, t_K = T, t_k \in \{2, \dots, T - 1\}, k = 2, \dots, K - 2$, which are unbiased observations of the true location:

$$(3.3) \quad Y(t_k) | \eta(t_k) \stackrel{\text{i.i.d.}}{\sim} N(\eta(t_k), \sigma_G^2),$$

for $k = 2, \dots, K - 2$. The known start and end points assumption implies that $Y(t_1) = \eta(t_1)$ and $Y(t_K) = \eta(t_K)$ are known.

Next, $X(t), t = 1, 2, \dots, T$ is used to denote the DR path without any error correction. To incorporate the bias of the DR path, we assume

$$(3.4) \quad X(t) = \eta(t) + h(t) + \xi(t),$$

where $h(t)$ is a parametric function designed to capture the systematic bias trend in the DR path. $\xi(t)$ denotes another Gaussian process independent of $\eta(t)$ that captures any irregular components in the deviation of the DR path from the truth:

$$\xi(1 : T) \sim N(\mathbf{0}, \mathbf{C}(1 : T, 1 : T)).$$

For the parametric bias component $h(t)$, we have considered various models, for example, $h(t) = \sum_{i=1}^Q \beta_i t^{i-1}$. The residual bias $\xi(t)$ is assumed to be a Brownian motion process (random walk of order 1) whose covariance function is therefore

$$C(s, t) = \sigma_D^2(\min(s, t) - 1).$$

We believe the Brownian motion process to be a reasonable approximation to the gradually accumulating error in the DRA. If we assume the errors in the velocity estimates from the DRA, after removing the systematic bias $h(t)$, at each time point are an i.i.d. normal sequence, the error in the integrated path is then a Brownian motion.

The final ingredients in our BM model are the prior distributions of the parameters. For notational simplicity, all densities are denoted by square brackets [...] throughout this paper. For σ_G^2 , we assume a known constant based on the previous extensive tests of the Fastloc®GPS device [Bryant (2007)]. The priors of the other two variance parameters are chosen to be $[\sigma_H^2] \propto 1/\sigma_H^2$ and $[\sigma_D^2] \propto 1/\sigma_D^2$, which are uniform priors on the log scale ($[\log(\sigma_H^2)] \propto 1$). For $\beta = (\beta_1, \beta_2, \dots, \beta_Q)^T$, a noninformative flat prior $[\beta] \propto 1$ is used. All these parameters are assumed to be independent of each other.

For expository simplicity in describing the joint distribution of all the data and parameters, the following notation is introduced:

- The unknown part of the true path is denoted by $\eta = \eta(2 : (T - 1))$, a $T - 2$ dimensional vector.
- GPS observations of the unknown part of the path are denoted by $Y = (Y(t_2), Y(t_3), \dots, Y(t_{k-1}))^T$, a $K - 2$ dimensional vector.
- The DR path is $\mathbf{X} = (\mathbf{X}(2 : (T - 1))^T, X(T) - Y(T))^T$, a vector of dimension $T - 1$.
- For the two unknown variance parameters, let $\phi = (\sigma_H^2, \sigma_D^2)^T$.

The joint likelihood of our model is

$$(3.5) \quad [\mathbf{X}, \mathbf{Y}, \eta, \beta, \phi] = [\phi][\beta][\eta|\phi][\mathbf{Y}|\eta][\mathbf{X}|\beta, \phi, \eta].$$

To obtain an estimate of the animal’s true path and its uncertainty, we need the posterior distribution

$$(3.6) \quad [\beta, \eta|\mathbf{X}, \mathbf{Y}] = \int \underbrace{[\beta, \eta|\mathbf{X}, \mathbf{Y}, \phi]}_{(1)} \times \underbrace{[\phi|\mathbf{X}, \mathbf{Y}]}_{(2)} d\phi.$$

Here we also include the β term, which can be used to assess the bias of the DRA. The posterior mean, denoted by $\tilde{\eta}(t)$, can be an estimate of the animal’s path and the posterior standard error, denoted by $\tilde{\sigma}(t)$, provides an uncertainty statement about the estimated path. The point-wise 95% credible interval for $\eta(t)$ can be constructed via a normal approximation,

$$(3.7) \quad [\tilde{\eta}(t) - 1.96\tilde{\sigma}(t), \tilde{\eta}(t) + 1.96\tilde{\sigma}(t)].$$

In principle, the “exact” credible intervals can be found via the normal mixtures in our numerical integration scheme, yet we found empirically in our case study that the exact credible intervals were almost indistinguishable from the normal approximated intervals in (3.7). This is discussed in detail in the supplementary material [Liu et al. (2016b)].

3.1. *Model inference.* To calculate the posterior (3.6), we first fix the variance parameters ϕ and calculate part (1) in equation (3.6) and then integrate over the posterior of ϕ . The first part of this section shows how the components of (3.6) can be efficiently evaluated. We then use numerical integration on an adaptive grid, same as in INLA [Rue, Martino and Chopin (2009)], to marginalize the randomness in ϕ . The numerical integration part is described in the supplementary material [Liu et al. (2016b)].

For notational simplicity, $\langle \cdot | \cdot \rangle$ denotes $[\cdot | \cdot, \phi]$, that is, $\langle \eta | \mathbf{X}, \mathbf{Y} \rangle = [\eta | \mathbf{X}, \mathbf{Y}, \phi]$. As we specify our model in a Gaussian and linear fashion, it is straightforward to show that $\langle \beta, \eta | \mathbf{X}, \mathbf{Y} \rangle$ is a multivariate Gaussian density,

$$(3.8) \quad \langle \beta, \eta | \mathbf{X}, \mathbf{Y} \rangle \propto \exp \left\{ -\frac{1}{2} \left((\zeta - \mathbf{M}_1^{-1} \mathbf{M}_2)^T \mathbf{M}_1 (\zeta - \mathbf{M}_1^{-1} \mathbf{M}_2) \right) \right\},$$

where $\zeta = (\beta^T, \eta^T)^T$ and $\mathbf{M}_1, \mathbf{M}_2$ are derived in the supplementary material [Liu et al. (2016b)].

Although the multivariate Gaussian posterior makes inference conceptually easy in implementation, calculating its posterior mean $\mathbf{M}_1^{-1} \mathbf{M}_2$ and covariance matrix \mathbf{M}_1^{-1} actually involves a matrix decomposition with computational complexity of order $O(T^3)$, which is a tremendous computational burden when T is large. It is possible to avoid the $O(T^3)$ matrix decomposition with certain sparse matrix techniques together with the Sherman–Morrison–Woodbury formula [Henderson and Searle (1981)], but those techniques still require the storage of some huge matrices and complicated matrix calculations. This pushes us to further reduce the complexity of (3.8).

It is easily seen that we have more information (data) about $\eta_G \triangleq \eta(t_{1:K})$ where the GPS observations are available than where they are not. For $\eta(1 : T \setminus t_{1:K})$, we only have the DR path. So our first step breaks η into two sets, that is,

$$(3.9) \quad \langle \beta, \eta | \mathbf{X}, \mathbf{Y} \rangle = \langle \eta(1 : T \setminus t_{1:K}) | \beta, \eta_G, \mathbf{X}, \mathbf{Y} \rangle \langle \beta, \eta_G, \mathbf{X}, \mathbf{Y} \rangle.$$

We can then use the Markovian property of the Brownian Bridge process [see e.g., Storzaker and Grimmett (2001)] to simplify (3.9) as

$$(3.10) \quad \langle \beta, \eta | \mathbf{X}, \mathbf{Y}, \phi \rangle = \left\{ \prod_{k=1}^{K-1} \langle \eta(t_k + 1 : t_{k+1} - 1) | \eta(t_k), \eta(t_{k+1}), \beta, \mathbf{X}, \mathbf{Y} \rangle \right\} \times \langle \beta, \eta_G | \mathbf{X}, \mathbf{Y} \rangle.$$

In this way, we partition the long η series into small pieces separated by the GPS observations. The next step exploits the Markovian property of the Brownian Motion and enables us to simplify the k th term in the first part of (3.10) as

$$(3.11) \quad \begin{aligned} &\langle \eta(t_k + 1 : t_{k+1} - 1) | \eta(t_k), \eta(t_{k+1}), \beta, \mathbf{X}, \mathbf{Y} \rangle \\ &= \langle \eta(t_k + 1 : t_{k+1} - 1) | \eta(t_k), \eta(t_{k+1}), \beta, \mathbf{X}(t_k : t_{k+1}) \rangle. \end{aligned}$$

All the derivations for (3.10) and (3.11) are provided in the supplementary material [Liu et al. (2016b)]. In (3.11), the posterior of $\eta(t)$ between two GPS points can be evaluated only with the corresponding DR path together with the posterior distribution of the two GPS points and β . This remarkably reduces the memory cost when computing the posterior of the long sequence and enables us to easily parallelize the whole calculation. Moreover, both the Brownian Bridge and Brownian Motion processes conditioned on two end points are Brownian Bridge processes, such that

$$\begin{aligned} \eta(t_k + 1 : t_{k+1} - 1) | \eta(t_k), \eta(t_{k+1}) &\sim \text{BB}(\eta(t_k), \eta(t_{k+1}), t_k, t_{k+1}, \sigma_H^2) \\ \xi(t_k + 1 : t_{k+1} - 1) | \xi(t_k), \xi(t_{k+1}) &\sim \text{BB}(\xi(t_k), \xi(t_{k+1}), t_k, t_{k+1}, \sigma_D^2). \end{aligned}$$

This fact is exploited to completely avoid the matrix inverse calculation when evaluating (3.11), which further reduces the computational burden. The derivations are included in the supplementary material [Liu et al. (2016b)]. Also, we found that the bias correction in the most simplified BM approach (empirical Bayesian, $\beta = 0$) is a shrinkage of the conventional bias correction, which will account for the signal-noise ratio in the DR path. A detailed discussion can be found in Liu et al. (2015).

However, the evaluation of $\langle \beta, \eta_G | \mathbf{X}, \mathbf{Y} \rangle$ in (3.10) still requires us to deal with the long sequence \mathbf{X} . But \mathbf{Y} is an unbiased observation of η_G , and therefore $\langle \eta_G | \mathbf{X}, \mathbf{Y} \rangle$ can be well approximated by $\langle \eta_G | \mathbf{Y} \rangle$. This approximation is exceptionally good when $\sigma_D^2 > \sigma_G^2$. For β , it can be well inferred from the difference between $\mathbf{X}_G \triangleq \mathbf{X}(t_{1:K})$ and \mathbf{Y} . Thus, we introduce the following approximation:

$$(3.12) \quad \langle \beta, \eta_G | \mathbf{X}, \mathbf{Y} \rangle \approx \langle \beta, \eta_G | \mathbf{X}_G, \mathbf{Y} \rangle.$$

With similar arguments, we can also approximate the posterior of ϕ by

$$(3.13) \quad [\phi | \mathbf{X}, \mathbf{Y}] \approx [\phi | \mathbf{X}_G, \mathbf{Y}].$$

The explicit expressions for (3.12) and (3.13) are included in the supplementary material [Liu et al. (2016b)]. Our simulations that mimic the real data sets have shown that the impact of the two approximation errors in (3.12) and (3.13) is negligible. We also verified through a thinned version of the real data set that the difference between the posterior obtained from (3.12) and (3.13) is not significant.

In summary, the posterior of η is approximated as follows:

$$\begin{aligned} [\eta, \beta | \mathbf{X}, \mathbf{Y}] &= \int [\eta, \beta | \mathbf{X}, \mathbf{Y}, \phi] [\phi | \mathbf{X}, \mathbf{Y}] d\phi \\ &= \int \langle \eta(1 : T \setminus t_{1:K}) | \beta, \eta_G, \mathbf{X}, \mathbf{Y} \rangle \langle \eta_G, \beta | \mathbf{X}, \mathbf{Y} \rangle [\phi | \mathbf{X}, \mathbf{Y}] d\phi \\ &= \int \left\{ \prod_{k=1}^{K-1} \langle \eta(t_k + 1 : t_{k+1} - 1) | \beta, \eta(t_k), \eta(t_{k+1}), \mathbf{X} \rangle \right\} \\ (3.14) \quad &\times \langle \eta_G, \beta | \mathbf{X}, \mathbf{Y} \rangle [\phi | \mathbf{X}, \mathbf{Y}] d\phi \end{aligned}$$

$$\begin{aligned}
 (3.15) \quad &= \int \left\{ \prod_{k=1}^{K-1} \langle \eta(t_k + 1 : t_{k+1} - 1) | \boldsymbol{\beta}, \eta(t_k), \eta(t_{k+1}), \mathbf{X}(t_k : t_{k+1}) \rangle \right\} \\
 &\quad \times \langle \boldsymbol{\eta}_G, \boldsymbol{\beta} | \mathbf{X}, \mathbf{Y} \rangle [\boldsymbol{\phi} | \mathbf{X}, \mathbf{Y}] d\boldsymbol{\phi} \\
 &\approx \int \left\{ \prod_{k=1}^{K-1} \langle \eta(t_k + 1 : t_{k+1} - 1) | \boldsymbol{\beta}, \eta(t_k), \eta(t_{k+1}), \mathbf{X}(t_k : t_{k+1}) \rangle \right\} \\
 &\quad \times \langle \boldsymbol{\eta}_G, \boldsymbol{\beta} | \mathbf{X}_G, \mathbf{Y} \rangle [\boldsymbol{\phi} | \mathbf{X}_G, \mathbf{Y}] d\boldsymbol{\phi}.
 \end{aligned}$$

The integration in equation (3.14) is calculated based on an adaptive grid based on $[\boldsymbol{\psi} | \mathbf{X}_G, \mathbf{Y}]$, which is discussed in the supplementary material [Liu et al. (2016b)]. Combining all these techniques to simplify computation reduces the computational time of our BM approach to a level similar to that of the DRA. For the two data sets we worked with, the DRA and BM of the DR path and GPS took less than five minutes in total on a regular laptop. We implemented the BM approach in an R package ‘‘BayesianAnimalTracker’’ [Liu (2014)]. The speed with which calculations can be done using this package [see Table 3 of Liu et al. (2015)] is a huge benefit for marine biologists who want to follow their animal while aboard a ship or on a remote island using a portable laptop without access to the Internet or any high performance computers.

4. Downscaling. Using the same notation as in the previous section, we propose the following downscaling model for the GPS observations and DR path:

$$(4.1) \quad Y(t_k) = \beta_0 + \gamma_1(t_k) + (\beta_1 + \gamma_2(t_k))X(t_k) + \varepsilon(t_k),$$

where $\gamma_1(t)$ and $\gamma_2(t)$ are zero-mean Gaussian processes, such as the random walks of order 1 and 2 (RW1, RW2) and autoregressive processes of order 1, 2 and 3 (AR1, AR2, AR3). Here $\varepsilon(t)$ is a white noise process. For expository simplicity, let $\boldsymbol{\gamma}$ denote all the unknown and random components in (4.1), including $\beta_0, \beta_1, \gamma_1(1 : T), \gamma_2(1 : T)$ and the hyperparameters governing them, for example, the variance/correlation parameters of $\gamma_1, \gamma_2, \varepsilon$. The combined path of the tracked animal can be learned from the posterior

$$\begin{aligned}
 &[Y(t) | X(t), \mathbf{X}(t_{1:K}), \mathbf{Y}(t_{1:K})] \\
 &= \int_{\boldsymbol{\gamma}} [Y(t), \boldsymbol{\gamma} | X(t), \mathbf{X}(t_{1:K}), \mathbf{Y}(t_{1:K})] d\boldsymbol{\gamma} \\
 &= \int_{\boldsymbol{\gamma}} [Y(t) | \boldsymbol{\gamma}, X(t), \mathbf{X}(t_{1:K}), \mathbf{Y}(t_{1:K})] [\boldsymbol{\gamma} | \mathbf{X}(t_{1:K}), \mathbf{Y}(t_{1:K})] d\boldsymbol{\gamma},
 \end{aligned}$$

for $t \in (1 : T) \setminus t_{1:K}$. Traditionally, the above integral has been calculated using an MCMC approach such as the Gibbs sampler [Berrocal, Gelfand and Holland (2010), Zidek, Le and Liu (2012)]. However, the MCMC approach is computationally expensive as well as technically challenging, and it sometimes encounters mixing or convergence problems. We therefore calculated the above posterior

by the integrated-nested Laplace approximation (INLA) via the R-INLA package [Martins et al. (2013)]. Basically, the INLA method seeks the posterior mode via numerical optimization, approximates the integrals of the random effects or hyperparameters via Laplace approximation, and numerically integrates over the hyperparameters on a selected grid based on the (approximated) likelihood. Readers may refer to papers by Rue, Martino and Chopin (2009) and Martins et al. (2013) for more detailed introductions of the INLA method.

For the downscaling approach, we use the default priors in R-INLA, which are all weakly informative priors. It is noteworthy that we do not put an informative prior on the variance parameter of $\varepsilon(t)$ as we do for the BM approach in equation (3.3) because $\varepsilon(t)$ represents not only the measurement error in $Y(t)$, but also the lack-of-fit errors of the downscaling model.

So far we have not found any direct equivalence between the BM and downscaling models, but notice that the posterior in both cases is essentially only calculated based on the DR path at the GPS observations $X(t_{1:K})$, not on the full set $X(1:T)$. This supports the use of our approximation to the likelihood in (3.12) and (3.13) from another perspective.

5. Simulation study. We performed several simulation studies to evaluate the performance of our approaches. These included a simulation to study the approximation in our BM approach (Section 5.1) and a comparison of all five approaches under three different data-generating models (Section 5.2).

5.1. Simulation to compare the approximation in the BM approach. We used a simulation to evaluate the impact of our likelihood approximation in (3.12) and (3.13). For expository reasons, let “full BM” denote the Bayesian Melding approach based on the full likelihood [left-hand side of (3.13)], and let “approximate BM” denote Bayesian Melding approach based on the approximate likelihood [right-hand side of (3.13)].

Here the data were generated according to our BM model: The true curve was simulated as a Brownian Bridge with $T = 2000$; the $K = 125$ GPS time points were randomly chosen from the $T = 2000$ time points; the GPS observations were i.i.d. normal observations of the true curve at these time points; the DR path was the true curve plus the bias function $h(t)$ and another Brownian Motion process. The parameters used in the simulation were the maximum likelihood estimates from our Trip 2 Northing data set. The results shown below are based on 1000 replicates. Similar findings were found from other settings and thus omitted.

The first two panels in Figure 2, include the box-whisker plots of the posterior mode of $\log(\sigma_H^2)$ and $\log(\sigma_D^2)$ from the full and approximate BM. As we used a uniform prior on the log scale, the posterior modes are equivalent to the maximum likelihood estimates based on either the full or the approximate likelihood. Both estimates were nearly unbiased in both parameters, but the approximate likelihood

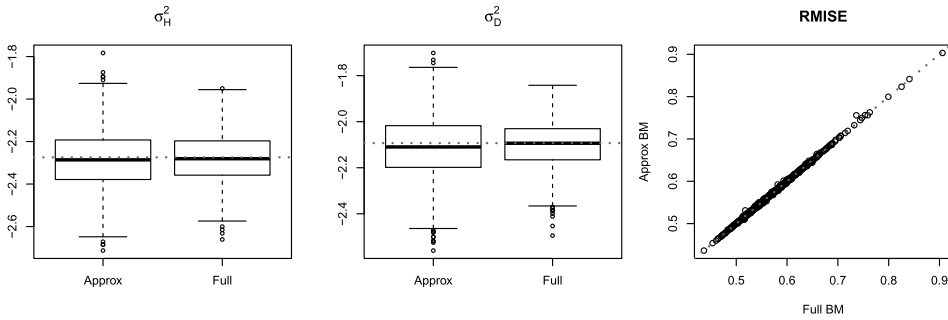


FIG. 2. Plots from our simulation, from left to right: the box plot of the posterior mode of $\log(\sigma_H^2)$ obtained from the approximate and full likelihoods; the box plot of the posterior modes of $\log(\sigma_D^2)$; scatter plot of the RMISE of the posterior mean of η from the approximate Bayesian Merging approach versus the RMISE of the posterior mean from the full Bayesian Merging approach.

estimates were obviously less efficient than the full likelihood estimates. The ratios between the standard errors of the approximate likelihood estimates and full likelihood estimates were 1.19 and 1.38 for $\log(\sigma_H^2)$ and $\log(\sigma_D^2)$, respectively. The increase in standard error, or, equivalently, the efficiency loss, was relatively small, as the approximate BM only uses a $(125 + 125)/(2000 + 125) = 2/17$ fraction of the observations used in the full BM for parameter inference. For example, if we assume the standard error of the estimates was proportional to $1/\sqrt{n}$ as in the i.i.d. case, the ratio between the standard errors would be predicted to be about $\sqrt{17/2} \approx 2.915$, far more than the ratio observed in the simulation study.

Moreover, the estimates of $\log(\sigma_H^2)$ and $\log(\sigma_D^2)$ are relatively unimportant, given that these are nuisance parameters in our Bayesian inference. What matters in the real application is the quality of the reconstructed path. Therefore, we calculated the root mean integrated squared error [RMISE, $\sqrt{\sum_{t=1}^T (\eta(t) - \bar{\eta}(t))^2 / T}$] between the true curve $\eta(t)$ and different estimates $\bar{\eta}(t)$. Here $\bar{\eta}(t)$ can generically represent the posterior distribution of $\eta(t)$ from either the full or approximate BM, or the posterior distribution of $Y(t)$ in the downscaling approach.

The third panel of Figure 2 is the scatter plot of the RMISE among all the replicates in our simulation. Clearly, most of the points lie on the diagonal line, indicating little difference between the reconstructed $\eta(t)$'s from approximate BM and full BM. This is because of the small efficiency loss in our likelihood approximation and the fact that we marginalize over the variance parameters in the posterior.

5.2. Comparison all five approaches. The above simulation study suggests that our approximate BM inference procedure is quite accurate. In the following simulation, we compared all the five candidate methods of estimating the animal's path: the two methods working with the GPS observations only (1. Linear interpolation and 2. CRAWL with drift term); and the three methods working with both

the GPS and DR path (3. Conventional bias correction of the DR path, 4. Our Bayesian Melding method, and 5. Our downscaling method). Here we only work with the approximate BM, as the full BM was very time consuming to run. The detailed model choices for the BM and downscaling were chosen to be the same as those selected for our real data application in the next section; that is, the BM model had the $h(t)$ as a constant and the downscaling model had both γ_1 and γ_2 as RW1.

The data were generated from three models: the Bayesian Melding model as mentioned above, the CRAWL model, and the downscaling model. When generating data from the CRAWL model, a path was first simulated from a CRAWL model fitted to the real data sets and the DR path was generated by adding a Brownian Motion to this path. In the downscaling model, we fixed the observed DR path (from the real data), and generated the GPS observations by our downscaling model. The parameter settings of all the data generation models were the estimates from our real data from Trip 2. One thousand replicates were generated from each model.

To summarize the performance in both dimensions, we report the pooled RMISE from both the northing and easting dimensions, namely,

$$\sqrt{\sum_{t=1}^T [(\eta_N(t) - \bar{\eta}_N(t))^2 + (\eta_E(t) - \bar{\eta}_E(t))^2] / (2 * T)},$$

where N stands for Northing and E stands for Easting dimensions. The pooled RMISE serves as a general measure of the goodness of approximation in both Northing and Easting dimensions. The box-plot of the RMISE in the two dimensions separately were similar and thus omitted. The box-plots of the pooled RMISE are in Figure 3. Our BM and downscaling methods have smaller RMISEs than all the other competitors regardless of which model the real path was generated from; that is, even if the animal’s path were generated from a CRAWL model (with an integrated OU process) instead of a Brownian Bridge, the BM approach with

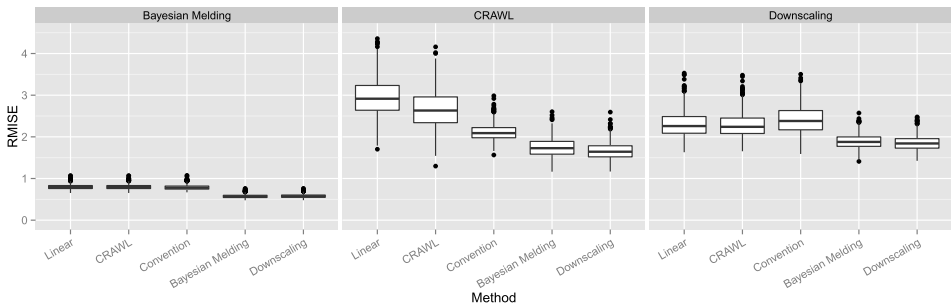


FIG. 3. Pooled RMISE for all five methods of estimating animal’s path, stratified by the data-generating model.

a misspecified prior still manages to outperform CRAWL interpolation with the high frequency DR path. In the comparison of BM and downscaling, their differences were very small. These findings were consistent with our findings in the cross-validation studies of the real data.

Another interesting finding is that the conventional bias correction of the DR path outperformed CRAWL when the data were generated from the CRAWL model but not when the data were generated by the downscaling model. This is because in the CRAWL data generation the error in the DR path is purely additive, while the error is both additive and multiplicative in the downscaling data generation. The conventional bias correction is only designed to deal with the additive error but not the multiplicative one. On the other hand, as the model parameters in the BM approach are adaptive in accordance with the observations, it still manages to predict the animal's path as well as the correctly specified downscaling model.

6. Case study results. We used our proposed BM and downscaling approaches to combine the DR path and GPS observations for high resolution paths of northern fur seals. To simplify computation and comparing different models, we thinned the original 16 Hz DR path (16 observations per second) into one observation per 5 minutes and added the GPS time points into this thinned time set. Notice here the thinning was done after the DR path was produced from the original 16 Hz data set. The resulting Trip 1 data set had 2100 time points, among which 274 were GPS time points. The resulting Trip 2 data set had 2334 time points, among which 130 were GPS time points. It is noteworthy that our BM approach could easily be fitted to the original "big" data sets based on the 1 Hz DR path (547,803 time points for Trip 1 and 661,249 for Trip 2). The results were reported in Liu et al. (2015). Individually modeling the two dimensions of the paths of the two animals yielded four data sets denoted as Trip 1 Northing (latitude), Trip 1 Easting (longitude), Trip 2 Northing and Trip 2 Easting, respectively.

We considered different bias functions $h(t)$ in our BM approach as well as different random processes γ_1, γ_2 for the downscaling approach. To compare these different models as well as the two approaches, we conducted leave-5-out cross-validation experiments (L5OCV) (removing 5 consecutive GPS observations at once when fitting our models) to evaluate the predictive ability of our models when the time gaps between the GPS observations are of relatively large size. Here we were less concerned with the model's predictive ability for short gaps, as there were natural constraints on the speed of our tracked animal. This means that when the time gaps were small, the animal's movements were confined in a small range and the performances of all methods were similar, that is, in leave-one-out cross-validations [Liu et al. (2015)]. L5OCV in our real data sets created gaps that would be longer than roughly 90% of the gaps in the observed GPS time points as shown in Table 1, and thus provided us with a good way to evaluate the long-term predictive performance. We used the root mean squared error (RMSE) as a measure for the prediction accuracy and also calculated the actual coverage percentage of

TABLE 2
RMSEs and actual coverage percentages of 95% credible intervals (in gray background) in L5OCV comparisons for different bias correction terms $h(t) = \sum_{i=1}^Q \beta_i t^{i-1}$ with $Q = 1, 2, 3, 4$ in the BM approach

	$Q = 1$		$Q = 2$		$Q = 3$		$Q = 4$	
Trip 1 Northing	0.80	94.9	0.80	95.2	0.80	95.6	0.80	95.6
Trip 1 Easting	0.75	97.8	0.75	98.2	0.76	97.8	0.76	97.8
Trip 2 Northing	3.06	93.0	3.06	93.0	2.73	92.2	2.83	89.1
Trip 2 Easting	2.62	96.9	2.60	96.1	2.52	93.8	2.53	89.8

the nominal 95% posterior credible intervals to examine whether the uncertainty in the combined path is calibrated properly.

In the rest of this section, we summarize the model selection results of the BM and downscaling models (Section 6.1 and 6.2, respectively). Then the cross-validation comparison with BM and downscaling approaches as well as linear interpolation, CRAWL, and conventional bias correction is in Section 6.3. The corrected path and its credible intervals for both methods are included in Section 6.4.

6.1. *Model selection for BM.* In our BM approach, we used the Brownian Bridge and Brownian Motion processes with different bias functions $h(t)$ in the DR path. Among many possible parameterizations of $h(t)$, we investigated only the polynomials $h(t) = \sum_{i=1}^Q \beta_i t^{i-1}$ of order $Q = 1$ (constant) to $Q = 4$. The RMSE and actual coverage are shown in Table 2.

As seen in Table 2, the BM with different $h(t)$ functions had very similar RMSE, that is, they differed little compared to the difference between the BM approach and the linear interpolation, etc., as in Table 5. The actual coverages of the credible intervals were reasonably close to the nominal 95% among the different Q 's. This indicates that increasing the complexity in $h(t)$ had little impact on the performance of our BM approach in our data sets. There was an exception, however, for the Trip 2 Northing direction where increasing Q to 3, 4 caused the CV-RMSE to increase, which came at the cost of lowering coverage percentages for the credible intervals. This observation led us to choose the simple BM approach with $Q = 1$ for further comparisons.

Perhaps our findings of little difference among the different BM models should not seem surprising, as we marginalized over the variance parameters σ_H^2, σ_D^2 and β [parameters in $h(t)$] when evaluating the posterior $[\eta|\mathbf{X}, \mathbf{Y}]$. That marginalization naturally helps to reduce the reliance on a good mean model to correct the bias in the DR path. Therefore, we chose not to pursue that investigation for more sophisticated parameterization of $h(t)$.

TABLE 3

Selected DIC values for the downscaling models. “NA” means that INLA crashed when fitting this model. The AR1–AR2 model minimizes the DIC for Trip 1 Northing, AR2–RW1 for Trip 1 Easting and Trip 2 Easting, and RW2–RW1 for Trip 2 Northing. The RW1–RW1 model is included as a benchmark

	RW1–RW1	RW2–RW1	AR1–AR2	AR2–RW1
Trip 1 Northing	–1608.41	–51.87	–1641.93	–1542.40
Trip 1 Easting	–487.04	–367.29	NA	–1683.86
Trip 2 Northing	–243.34	–853.31	–729.44	–827.04
Trip 2 Easting	–774.80	–91.57	–741.25	–829.27

6.2. *Model selection for downscaling.* For the downscaling model (4.1), we considered random walks of order 1 and 2 (RW1, RW2) and autoregressive processes of order 1, 2, 3 (AR1, AR2, AR3) for both $\gamma_1(t)$ and $\gamma_2(t)$, leading to 25 models in total. They are denoted in “XXX–YYY” form (i.e., RW1–AR2 denotes the downscaling model with γ_1 as a random walk of order 1 and γ_2 as an autoregressive process of order 2). Not every model fit our data sets well and INLA crashed due to numerical issues when fitting certain models. It was not feasible with our computational resources to perform cross-validation for all of the 25 models. Instead, we screened these models using the conventional deviance information criterion [DIC, Spiegelhalter et al. (2002)], which can also be calculated by the INLA package. We found that the DIC was minimized by some simple models for our data sets and have listed the DIC values for them together with the simplest RW1–RW1 model in Table 3.

None of the models involving AR3 components were selected by the DIC criterion, indicating that the dependence in the two random processes were of short memory, that is, they only depended on the previous two time points. Also, it is clear from Table 3 that none of these models dominated in all four data sets. The RW2–RW1 model achieved the smallest DIC in the two Easting data sets, but it did not fit well in the Trip 1 Northing. However, the simplest RW1–RW1 model achieved reasonable fit in all of the four data sets, and thus was included in the following comparisons.

As pointed out by Spiegelhalter et al. (2014), DIC is not an ideal criterion for the predictive power of the models, which was our key objective in reconstructing the animal’s path. We further compared the four downscaling models via a leave-5-out cross-validation and summarized the results in Table 4. Among the four downscaling models we considered, AR2–RW1 and AR1–AR2 were the first to be ruled out, as they had large prediction errors in the Trip 2 Northing and Easting data sets. Close examination of the cross-validation results found they completely failed to correct the DR path for a certain period of the trip and resulted in errors as large as 100 km. In addition, the credible intervals for AR2–RW1 and AR1–AR2 failed to achieve the nominal coverage percentage for Trip 1 Northing or Trip 2 Easting. As

TABLE 4

RMSEs and actual coverage percentages of nominally 95% credible intervals (in gray background) for the LSOVC comparisons of the different downscaling models with different processes

		Downscaling with different γ_1, γ_2			
		RW1–RW1	RW2–RW1	AR1–AR2	AR2–RW1
Trip 1 Northing	RMSE (km)	0.95	0.83	1.06	2.73
	Coverage (%)	95.6	91.5	94.9	86.0
Trip 1 Easting	RMSE (km)	0.75	0.93	0.71	0.80
	Coverage (%)	98.9	95.2	96.3	96.6
Trip 2 Northing	RMSE (km)	2.59	1.61	3.56	5.26
	Coverage (%)	93.0	98.4	92.9	91.1
Trip 2 Easting	RMSE (km)	2.56	4.08	18.27	18.32
	Coverage (%)	98.4	93.8	85.2	96.1

for the comparison between the RW2–RW1 and RW1–RW1 models, RW2–RW1 had slightly smaller RMSEs in the two Easting data sets, while RW1–RW1 had smaller RMSEs in the two Northing data sets. Yet these two models in general achieved similar performances in terms of the RMSE and actual coverage percentage. We therefore chose the simpler RW1–RW1 model for further comparisons.

6.3. *Cross-validation comparison of the different approaches.* We compared the selected BM model with $Q = 1$ (BM1 for short) and downscaling the RW1–RW1 model (DS11 for short) with the competitors: linear interpolation, conventional bias correction, and CRAWL [Johnson et al. (2008)]. Linear interpolation provided the same mean curve as using the Brownian Bridge to interpolate the GPS observations. CRAWL interpolated the GPS observations via state-space models, whose process model is an integrated Ornstein–Uhlenbeck process with a drift term (but assuming the correlation and process noise parameters are the same in both dimensions). Linear interpolation and CRAWL were based on the GPS observations only. Conventional bias correction was previously described in (2.1). The CV–RMSE and coverage percentages of the credible intervals are summarized in Table 5.

We first compared the two approaches only with the GPS observations (first two columns of Table 5) to the approaches that combined both the GPS observations and DR path (the last three columns of Table 5). We found that the latter approaches had better prediction performance in general, which demonstrates the great value of the DR path in providing fine-scale details of the animal’s movement. In the comparison of linear interpolation and CRAWL, the more complex CRAWL had a larger RMSE than linear interpolation in the two Easting data sets we considered, which indicates a poor fit for the CRAWL models. In addition, the coverage percentages of CRAWL were lower than the nominal level in the two data sets from Trip 2.

TABLE 5

RMSEs and actual coverage percentages of nominally 95% credible intervals (in gray background) for the L5OCV comparisons of all the approaches. Two approaches that only use GPS data: Linear interpolation (Linear) and Correlated Random Walk (CRAWL) with drift term. Three approaches use both GPS and DR path: conventional bias correction of DR (Convention), Bayesian Melding with $Q = 1$ (BM1), and Downscaling with RW1–RW1 model (DS11)

		Linear	CRAWL	Convention	BM1	DS11
Trip 1 Northing	RMSE (km)	1.16	1.12	1.25	0.80	0.95
	Coverage (%)		94.1		94.9	95.6
Trip 1 Easting	RMSE (km)	1.13	1.28	1.04	0.75	0.75
	Coverage (%)		93.8		97.8	98.9
Trip 2 Northing	RMSE (km)	4.44	3.70	3.33	3.06	2.59
	Coverage (%)		88.3		93.0	93.0
Trip 2 Easting	RMSE (km)	3.84	3.98	2.67	2.62	2.56
	Coverage (%)		90.6		96.9	98.4

We also noticed that the conventional approach had a larger RMSE than linear interpolation with the Trip 1 Northing data set, which shows that the conventional approach failed to properly use the high resolution DR path. The same issue was not found with our BM and downscaling approaches, both of which achieved a smaller RMSE than the other three approaches uniformly in all the four data sets we considered. Also, the reduction in the RMSE achieved by our BM or downscaling approaches was larger than the differences between the BM or downscaling approaches with different model components as shown in Tables 2 and 4.

In the comparison between the selected BM and downscaling models (last two columns of Table 5), the BM1 had a smaller RMSE for Trip 1 Northing while the DS11 had a smaller RMSE for the Trip 2 Northing. They achieved similar RMSEs in the two Easting data sets. They also had similar coverage percentages across all four data sets. Thus, we could not see any noteworthy differences in the performance of the BM and downscaling approaches.

To further explain the results in Table 5, we plotted the corrected path for all five approaches considered above and zoomed in on the time period 12:00–24:00 for 2009-07-23 in Trip 1 to better illustrate their differences (Figure 4). From this plot, we see that the conventional corrected path went through the GPS observations directly as did the linear interpolation, but it inferred dramatic changes between the GPS observations. The reconstructed path from BM and downscaling aligned well with the GPS observations while retaining detail from the conventional bias correction. Liu et al. (2015) show that the BM corrected path shrinks the conventional bias correction toward that of the linear interpolation. This shrinkage removes the noise in the DR path in a statistical way and gives the BM an advantage over the conventional approach. From this plot, we also found that the corrected path from BM and downscaling were very close.

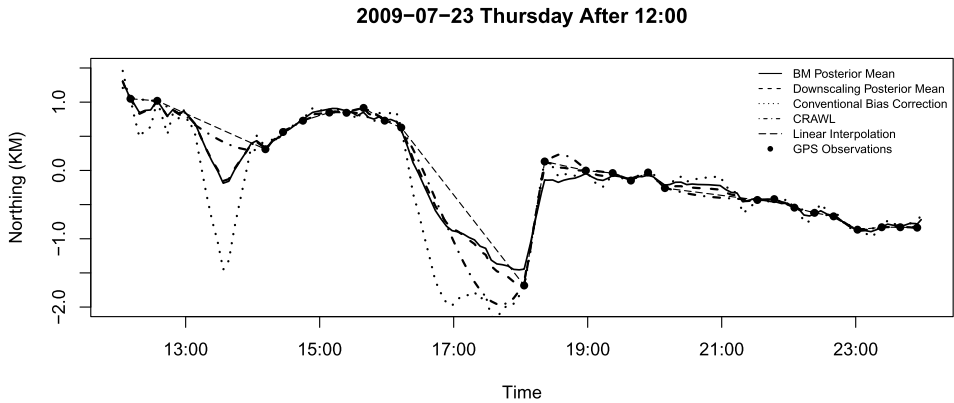


FIG. 4. *The reconstructed path for a northern fur seal in a selected period from all the five approaches considered in our study, Bayesian Melding (BM), Downscaling (DS11), Conventional bias correction, CRAWL and linear interpolation. The dots are the GPS observations.*

However, the path from CRAWL showed some unrealistic trends, like the up-swing before 19:00, while the DR path indicated that the animal was moving in the opposite direction. These unrealistic trends likely resulted from the model assumptions in CRAWL, which may not fit the data well. These unrealistic trends and the resulting poor performance of CRAWL in cross-validations seem to have derived from the lack of fine detail provided by the DRA.

6.4. *Combined path and its uncertainty from BM and downscaling.* Figure 4 only covered a small period of our data. We applied our proposed BM and downscaling approaches to the four data sets and found they all successfully corrected the bias of the DR path and properly quantified the uncertainty. We therefore only present the plots for the corrected path for the Trip 1 Northing data set. Similar plots and analysis were found in the other three data sets and are thus omitted. In Figure 5, we show the corrected path from the BM (solid curve) and downscaling (dotted curve) approaches, which are the posterior mean of $\eta(t)$ when BM was used, and $Y(t)$ when the downscaling approach was used. The point-wise 95% credible intervals (gray solid curve for BM and purple dotted curve for downscaling) were included to represent the uncertainty around the corrected path. We also included the original data—GPS observations (round points) and the DR path (dashed curve), from which it is clear that the bias of the DRA grew dramatically over time and reached 100 km at the end of this trip. The location estimate in the DR path was not very useful in predicting the animal's location, but the fluctuations in the DR path matched the fluctuations of the GPS observations, meaning that the DR path has useful high-frequency information that can be further exploited to fill in the gaps between GPS observations. This was successfully achieved by our proposed BM and downscaling approaches, as the corrected path from both approaches lay close to the GPS observations.

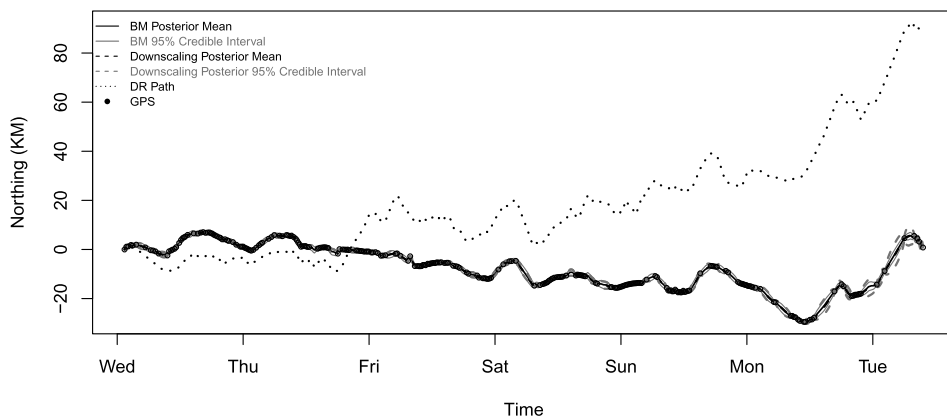


FIG. 5. *The Bayesian Melding and downscaling results for a northern fur seal undertaking Trip 1 Northing from Bogoslof Island, Alaska: Points are the GPS observations and the dotted curve is the DR path. The solid curve is the posterior mean of $\eta(t)$ in the case of BM, whose 95% credible intervals are shown by the gray solid curve. The dotted curve is the posterior mean of $Y(t)$ in the downscaling approach, whose 95% credible intervals are shown by the gray dotted curve.*

For the scale of Figure 5, the corrected path and CIs from BM and downscaling were almost indistinguishable. To show how our approaches worked in a fine scale, we zoomed into the Day 2 (2009–07–23) and Day 6 (2009–07–27) part of this trip. We can confirm from Figure 6 that the corrected paths from the two approaches were similar, as the curves of the posterior means nearly overlaid each other. As well, the CIs from both approaches displayed a clear “bridge” structure, that is, they were narrower at the GPS time points and wider in between the GPS observations. This is plausible, as we have direct and accurate observations at the GPS time points and less accurate information when the GPS locations were not available. The error grows as the track moves away from the GPS observations and decreases near the next GPS observation. Also, the longer the gap between the GPS time points, the larger the error and thus the wider credible intervals, which is seen on comparing Days 2 and 6. On Day 6, fewer GPS observations were available and the gaps were longer, which resulted in overall wider credible intervals.

Another interesting finding seen in Figure 6 is that the CI from the downscaling approach was narrower than those from BM on Day 2 while they were wider on Day 6. This was caused by the two RW1 components in the downscaling model, as their variance was growing with time (Figure 7). On the other hand, the posterior SD for the BM approach was more stable, as it was more constrained with the Brownian Bridge structure.

7. Concluding remarks. We present a Bayesian Melding approach and a downscaling approach to combine sparse but accurate GPS observations with high resolution but biased DR paths for the tracking of marine mammals. The posterior

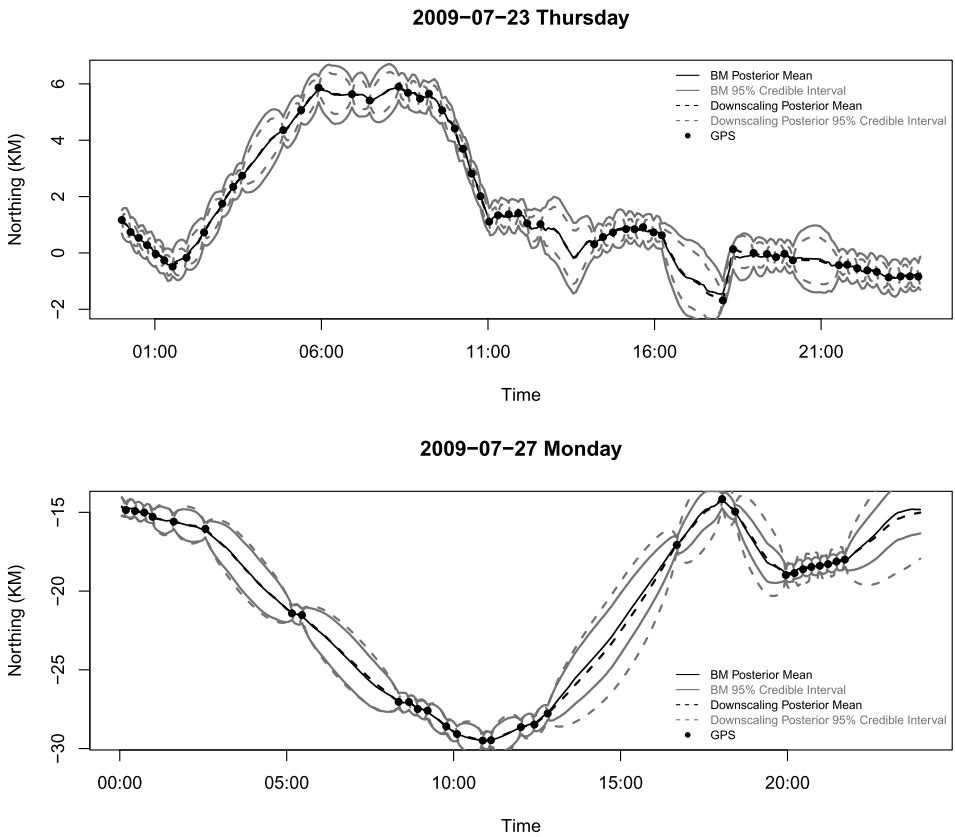


FIG. 6. Zoomed Bayesian Melding and downscaling results for a northern fur seal undertaking Trip 1 Northing on 2009-07-23 and 2009-07-27: Red points are the GPS observations. The solid curve is the posterior mean of $\eta(t)$ in BM, whose 95% credible intervals are shown by the gray solid curve. The dotted curve is the posterior mean of $Y(t)$ in downscaling, whose 95% credible intervals are shown by the gray dotted curve.

mean from our BM and downscaling approaches both offer an accurate and high resolution path for the tracked animals and the posterior credible intervals provide a reasonable statement of the uncertainty in our inferences. The good predictive performance of our approaches is also supported by our simulation studies. Moreover, neither of our methods requires computationally expensive MCMC methods for computation. Our BM approach exploits the conditional independence property of the Brownian Bridge and Brownian Motion to dramatically reduce the heavy computational burden involved in dealing with large data sets. The downscaling approach is fitted via the computationally efficient INLA approach. The quality of the likelihood approximation in BM and correctness of downscaling were confirmed in our simulation study.

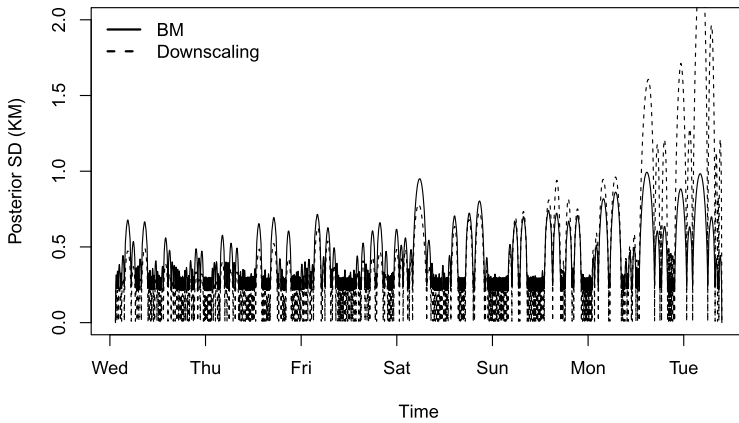


FIG. 7. Posterior standard deviation (SD) from Bayesian Melding and downscaling results for a northern fur seal undertaking Trip 1 Northing. The solid curve is from BM, while the dotted curve is from downscaling.

We performed cross-validation studies to compare different models in these two approaches and found that the prediction performance of the simplest approaches (i.e., BM with a constant bias term and downscaling with both two random effects being first order random walks) were as good as or even better than those of the more complex models, according to our empirical assessments. This finding is partially explained by the fact that we marginalized over the model parameters in the posterior distribution for our tracked subjects. In the comparison between BM and downscaling, we could not find any noteworthy differences between these two approaches in their prediction accuracy and actual coverage percentage of their credible intervals. However, our implementation of BM is better because it is more scalable to big data sets with more than half a million time points on a regular computer [Liu et al. (2015)], while the downscaling approach fitted by INLA can only work with thinned data sets on the same computer. Also, we built BM on a process that reflects the nature of our tracked subject, making it superior for future development of our theory.

McClintock et al. (2014) have shown many disadvantages of using a discrete time formulation when working with satellite data, which may lead one to question the discrete time formulation we used, yet animal movement (e.g., the fur seals we tracked) is ultimately powered by its body movement (e.g., the stroking of flippers), and there is a maximum frequency of body movement that an animal is capable of achieving. Therefore, the animal's movement is essentially discrete and can thus be sufficiently well described by a discrete process model with an observation frequency of no less than twice the maximum frequency of the animal's body movement [Nyquist frequency, see, e.g., Le and Zidek (2006)]. The Nyquist frequency was taken into consideration in data collection, that is, the original sampling frequency of the DR path was 16 Hz in our northern fur seal data.

The DR path thus captures the fine detail in an animal's movements and provides observations of the animal's path in "continuous time" with respect to the animal. Our discrete time formulation in Bayesian Melding or downscaling is thus backed up by these "continuous time" observations, which are free of the shortcomings of discrete time models for satellite data.

One concern about our Brownian Bridge prior in the Bayesian Melding approach is that the GPS observations (Figure 1) appear to be much smoother than a Brownian Bridge process, yet it is important to recognize that the Brownian Bridge is only a prior distribution for the animal's path. The corrected path, as seen in Figure 6, retains the smoothness and does not become wiggly as a simulated Brownian Bridge because the corrected path is posterior given both the GPS and DR paths. The smoothness of the DR path is preserved in the posterior. However, our BM approach can undoubtedly be further improved by replacing the Brownian Bridge process prior with some other processes that reflect more features of the animal's movements, such as a Brownian Bridge process with dynamic variance, the integrated Ornstein–Uhlenback process as in [Johnson et al. \(2008\)](#), or a solution to a stochastic differential equation that describes the animal's habitat preference. This is being addressed in our future work.

The modeling approaches we developed and tested can facilitate the processing of a high resolution in situ record of the hydrographic data collected by marine mammals, and can contribute to broadening knowledge about parts of the ocean that have been hard to observe. They can contribute to studies seeking to address the effects of climate change on the ocean, and also contribute to answering many biological and ecological questions about habitat preference and resource selection [[Hooten et al. \(2013\)](#)].

Our work also demonstrates the value of using the Bayesian data fusion techniques to combine observations from different sources for tracking objects. We are currently working on adapting the ideas developed in this paper to track basketball players as well as the progress of infectious disease. For the latter case, we are using the Google flu trends data as a biased but high resolution source of observations and Center for Disease Control (CDC) reports as an accurate but sparse set of observations. The bias and failure to predict some disease epidemics by Google flu have been studied in [Lazer et al. \(2014a, 2014b\)](#) and the references within. The media also used it as a serious warning about the use of "big data," as noted by [Salzberg \(2014\)](#) who commented: "Big data can be great, but not when it is bad data." While agreeing with this comment in principle, we would point out that "bad big data," such as the Google flu trend or the DR path in our paper, can be good again in cases when it can be combined and corrected by good data. So, for example, [Dugas et al. \(2013\)](#) and [Lazer et al. \(2014a\)](#) used various regression models to combine the Google flu and CDC reports and achieved better predictions for infectious disease. Our BM and downscaling approaches also successfully combine the DR path with GPS observations.

Acknowledgements. The northern fur seal data were collected as part of the BEST-BSIERP “Bering Sea Project” funded jointly by the US National Science Foundation and the North Pacific Research Board. Additional support was provided by the North Pacific Universities Marine Mammal Research Consortium through the North Pacific Marine Science Foundation. Data collection was done under the National Oceanographic and Atmospheric Administration (NOAA) permit no. 14329 and abided by the guidelines of the Committee on Animal Care at the University of British Columbia (permit no. A09-0345). We are indebted to the Editor and three referees for their constructive criticisms on earlier versions of our manuscript.

SUPPLEMENTARY MATERIAL

Supplement to “Bayesian data fusion approaches to predicting spatial tracks: Application to marine mammals” (DOI: [10.1214/16-AOAS945SUPP](https://doi.org/10.1214/16-AOAS945SUPP.pdf); .pdf). *Supplement A*: Details of the dead-reckoning algorithm. We provide additional details of the Dead-Reckoning Algorithm to help understand how it works and why it is biased.

Supplement B: Details of Bayesian melding. This supplement includes the detailed derivations of the inferential methods needed for our Bayesian Melding approach. It includes the following subsections:

1. Explicit form of $\langle \boldsymbol{\beta}, \boldsymbol{\eta} | \mathbf{X}, \mathbf{Y} \rangle$.
2. Derivation of (3.10) and (3.11).
3. Explicit expression for (3.11).
4. Explicit expression of $[\boldsymbol{\phi}, \boldsymbol{\beta}, \boldsymbol{\eta}_G | \mathbf{X}_G, \mathbf{Y}]$.
5. Marginal distribution of $\boldsymbol{\eta}$ at the non-GPS points.
6. Integration over the variance parameters $\boldsymbol{\phi}$.
7. The goodness of normal approximation credible intervals.

Supplement C: Figures in color. The colored version of Figures 1, 4, 5 and 6.

REFERENCES

- BATTAILE, B. (2014). TrackReconstruction: Reconstruct animal tracks from magnetometer, accelerometer, depth and optional speed data. R package version 1.1.
- BATTAILE, B. C., NORDSTROM, C. A., LIEBSCH, N. and TRITES, A. W. (2015). Foraging a new trail with northern fur seals (*Callorhinus ursinus*): Lactating seals from islands with contrasting population dynamics have different foraging strategies, and forage at scales previously unrecognized by GPS interpolated dive data. *Marine Mammal Science* **31** 1494–1520.
- BENOIT-BIRD, K. J., BATTAILE, B. C., HEPPELL, S. A., HOOVER, B., IRONS, D., JONES, N., KULETZ, K. J., NORDSTROM, C. A., PAREDES, R., SURYAN, R. M., WALUK, C. M. and TRITES, A. W. (2013a). Prey patch patterns predict habitat use by top marine predators with diverse foraging strategies. *PLoS ONE* **8** e53348.
- BENOIT-BIRD, K. J., BATTAILE, B. C., NORDSTROM, C. A. and TRITES, A. W. (2013b). Foraging behavior of northern fur seals closely matches the hierarchical patch scales of prey. *Mar. Ecol. Prog. Ser.* **479** 283–302.

- BERROCAL, V. J., GELFAND, A. E. and HOLLAND, D. M. (2010). A spatio-temporal downscaler for output from numerical models. *J. Agric. Biol. Environ. Stat.* **15** 176–197. [MR2787270](#)
- BLOCK, B. A., JONSEN, I. D., JORGENSEN, S. J., WINSHIP, A. J., SHAFFER, S. A., BOGRAD, S. J., HAZEN, E. L., FOLEY, D. G., BREED, G. A., HARRISON, A.-L., GANONG, J. E., SWITENBANK, A., CASTLETON, M., DEWAR, H., MATE, B. R., SHILLINGER, G. L., SCHAEFER, K. M., BENSON, S. R., WEISE, M. J., HENRY, R. W. and COSTA, D. P. (2011). Tracking apex marine predator movements in a dynamic ocean. *Nature* **475** 86–90.
- BOEHME, L., KOVACS, K. and LYDERSEN, C. (2010). Biologging in the global ocean observing system. *Proceedings of OceanObs 09: Sustained Ocean Observations and Information for Society* **2** 21–25.
- BOEHME, L., MEREDITH, M. P., THORPE, S. E., BIUW, M. and FEDAK, M. (2008). Antarctic circumpolar current frontal system in the South Atlantic: Monitoring using merged Argo and animal-borne sensor data. *Journal of Geophysical Research C: Oceans* **113** C9.
- BRYANT, E. (2007). 2D Location Accuracy Statistics for Fastloc RCores Running Firmware Versions 2.2 and 2.3. Wildtrack Telemetry Systems Ltd.
- DUGAS, A. F., JALALPOUR, M., GEL, Y., LEVIN, S., TORCASO, F., IGUSA, T. and ROTHMAN, R. E. (2013). Influenza forecasting with Google Flu Trends. *PLoS ONE* **8** e56176.
- DUKIC, V., LOPES, H. F. and POLSON, N. G. (2012). Tracking epidemics with Google Flu Trends data and a state-space SEIR model. *J. Amer. Statist. Assoc.* **107** 1410–1426. [MR3036404](#)
- ELKAIM, G. H., DECKER, E. B., OLIVER, G. and WRIGHT, B. (2006). Marine Mammal Marker (MAMMARK) dead reckoning sensor for in-situ environmental monitoring. *Proceedings of the ION/IEEE PLANS* 976–987.
- FLEMING, C. H., FAGAN, W. F., MUELLER, T., OLSON, K. A., LEIMGRUBER, P. and CALABRESE, J. M. (2016). Estimating where and how animals travel: An optimal framework for path reconstruction from autocorrelated tracking data. *Ecology*.
- FOLEY, K. M. and FUENTES, M. (2008). A statistical framework to combine multivariate spatial data and physical models for hurricane surface wind prediction. *J. Agric. Biol. Environ. Stat.* **13** 37–59. [MR2423075](#)
- FUENTES, M. and RAFTERY, A. E. (2005). Model evaluation and spatial interpolation by Bayesian combination of observations with outputs from numerical models. *Biometrics* **61** 36–45. [MR2129199](#)
- GINSBERG, J., MOHEBBI, M. H., PATEL, R. S., BRAMMER, L., SMOLINSKI, M. S. and BRILLIANT, L. (2009). Detecting influenza epidemics using search engine query data. *Nature* **457** 1012–1014.
- HENDERSON, H. V. and SEARLE, S. R. (1981). On deriving the inverse of a sum of matrices. *SIAM Rev.* **23** 53–60. [MR0605440](#)
- HOOTEN, M. B., HANKS, E. M., JOHNSON, D. S. and ALLDREDGE, M. W. (2013). Reconciling resource utilization and resource selection functions. *J. Anim. Ecol.* **82** 1146–1154.
- HORNE, J. S., GARTON, E. O., KRONE, S. M. and LEWIS, J. S. (2007). Analyzing animal movements using Brownian bridges. *Ecology* **88** 2354–2363.
- HUMPHRIES, N. E., QUEIROZ, N., DYER, J. R. M., PADE, N. G., MUSYL, M. K., SCHAEFER, K. M., FULLER, D. W., BRUNNSCHWEILER, J. M., DOYLE, T. K., HOUGHTON, J. D. R., HAYS, G. C., JONES, C. S., NOBLE, L. R., WEARMOUTH, V. J., SOUTHALL, E. J. and SIMS, D. W. (2010). Environmental context explains Lévy and Brownian movement patterns of marine predators. *Nature* **465** 1066–1069.
- JOHNSON, M. P. and TYACK, P. L. (2003). A digital acoustic recording tag for measuring the response of wild marine mammals to sound. *IEEE Journal of Oceanic Engineering* **28** 3–12.
- JOHNSON, D. S., LONDON, J. M., LEA, M.-A. and DURBAN, J. W. (2008). Continuous-time correlated random walk model for animal telemetry data. *Ecology* **89** 1208–1215.
- JONSEN, I. D., FLEMMING, J. M. and MYERS, R. A. (2005). Robust state-space modeling of animal movement data. *Ecology* **86** 2874–2880.

- KRANSTAUBER, B., SAFI, K. and BARTUMEUS, F. (2014). Bivariate Gaussian bridges: Directional factorization of diffusion in Brownian bridge models. *Mov. Ecol.* **2** 5.
- KRANSTAUBER, B., KAYS, R., LAPOINT, S. D., WIKELSKI, M. and SAFI, K. (2012). A dynamic Brownian bridge movement model to estimate utilization distributions for heterogeneous animal movement. *J. Anim. Ecol.* **81** 738–746.
- LAZER, D., KENNEDY, R., KING, G. and VESPIGNANI, A. (2014a). Big data. The parable of Google Flu: Traps in big data analysis. *Science* **343** 1203–1205.
- LAZER, D., KENNEDY, R., KING, G. and VESPIGNANI, A. (2014b). Google Flu Trends still appears sick: An evaluation of the 2013–2014 Flu season. *SSRN Electronic Journal* 1–11.
- LE, N. D. and ZIDEK, J. V. (2006). *Statistical Analysis of Environmental Space–Time Processes*. Springer, New York. [MR2223933](#)
- LINDGREN, F., RUE, H. and LINDSTRÖM, J. (2011). An explicit link between Gaussian fields and Gaussian Markov random fields: The stochastic partial differential equation approach. *J. R. Stat. Soc. Ser. B. Stat. Methodol.* **73** 423–498. [MR2853727](#)
- LIU, Y. (2014). *BayesianAnimalTracker: Bayesian Melding of GPS and DR Path for Animal Tracking*. R package version 1.2.
- LIU, Z., LE, N. D. and ZIDEK, J. V. (2011). An empirical assessment of Bayesian melding for mapping ozone pollution. *Environmetrics* **22** 340–353. [MR2843389](#)
- LIU, Y., BATTAILE, B. C., ZIDEK, J. V. and TRITES, A. W. (2015). Bias correction and uncertainty characterization of dead-reckoned paths of marine mammals. *Animal Biometrics* **3** 51.
- LIU, Y., DINSDALE, D. R., JUN, S.-H., BRIERCLIFFE, C. and BONE, J. (2016a). Automatic learning of basketball strategy via SportVU tracking data: The potential field approach. *Cascadia Symposium on Statistics in Sports*, Vancouver.
- LIU, Y., ZIDEK, J. V., TRITES, A. W. and BATTAILE, B. C., (2016b). Supplement to “Bayesian data fusion approaches to predicting spatial tracks: Application to marine mammals.” DOI:10.1214/16-AOAS945SUPP.
- MARTINS, T. G., SIMPSON, D., LINDGREN, F. and RUE, H. (2013). Bayesian computing with INLA: New features. *Comput. Statist. Data Anal.* **67** 68–83. [MR3079584](#)
- MCCCLINTOCK, B. T., JOHNSON, D. S., HOOTEN, M. B., VER HOEF, J. M. and MORALES, J. M. (2014). When to be discrete: The importance of time formulation in understanding animal movement. *Mov. Ecol.* **2** 1–14.
- MILLER, A., BORNN, L., ADAMS, R. and GOLDSBERRY, K. (2014). Factorized point process intensities: A spatial analysis of professional basketball. Preprint. Available at [arXiv:1401.0942](#).
- MITANI, Y., SATO, K., ITO, S., CAMERON, M. F., SINIFF, D. B. and NAITO, Y. (2003). A method for reconstructing three-dimensional dive profiles of marine mammals using geomagnetic intensity data: Results from two lactating Weddell seals. *Polar Biology* **26** 311–317.
- NORDSTROM, C. A., BENOIT-BIRD, K. J., BATTAILE, B. C. and TRITES, A. W. (2013). Northern fur seals augment ship-derived ocean temperatures with higher temporal and spatial resolution data in the eastern Bering Sea. *Deep Sea Research Part II* **94** 257–273.
- POZDNYAKOV, V., MEYER, T., WANG, Y.-B. and YAN, J. (2014). On modeling animal movements using Brownian motion with measurement error. *Ecology* **95** 247–253.
- RUE, H., MARTINO, S. and CHOPIN, N. (2009). Approximate Bayesian inference for latent Gaussian models by using integrated nested Laplace approximations. *J. R. Stat. Soc. Ser. B. Stat. Methodol.* **71** 319–392. [MR2649602](#)
- RUNDEL, C. W., SCHLIEP, E. M., GELFAND, A. E. and HOLLAND, D. M. (2015). A data fusion approach for spatial analysis of speciated PM_{2.5} across time. *Environmetrics*.
- SACKS, J., WELCH, W. J., MITCHELL, T. J. and WYNN, H. P. (1989). Design and analysis of computer experiments. *Statist. Sci.* **4** 409–435. [MR1041765](#)
- SAHU, S. K., GELFAND, A. E. and HOLLAND, D. M. (2010). Fusing point and areal level space-time data with application to wet deposition. *J. R. Stat. Soc. Ser. C. Appl. Stat.* **59** 77–103. [MR2750133](#)

- SALZBERG, S. (2014). Why Google flu is a failure. *Forbes.com* [online] 03–24.
- SAWYER, H., KAUFFMAN, M. J., NIELSON, R. M. and HORNE, J. S. (2009). Identifying and prioritizing ungulate migration routes for landscape-level conservation. *Ecological Applications* **19** 2016–2025.
- SPIEGELHALTER, D. J., BEST, N. G., CARLIN, B. P. and VAN DER LINDE, A. (2002). Bayesian measures of model complexity and fit. *J. R. Stat. Soc. Ser. B. Stat. Methodol.* **64** 583–639. [MR1979380](#)
- SPIEGELHALTER, D. J., BEST, N. G., CARLIN, B. P. and VAN DER LINDE, A. (2014). The deviance information criterion: 12 years on. *J. R. Stat. Soc. Ser. B. Stat. Methodol.* **76** 485–493. [MR3210727](#)
- STIRZAKER, G. G. D. and GRIMMETT, D. (2001). *Probability and Random Processes*. Oxford Science Publications, Oxford.
- WAHBA, G. (1965). A least squares estimate of satellite attitude. *SIAM Rev.* **7** 409–409.
- WILSON, R. P. and WILSON, M. P. (1988). Dead reckoning—a new technique for determining penguin movements at sea. *Meeresforschung—Reports on Marine Research* **32** 155–158.
- WILSON, R. P., LIEBSCH, N., DAVIES, I. M., QUINTANA, F., WEIMERSKIRCH, H., STORCH, S., LUCKE, K., SIEBERT, U., ZANKL, S., MÜLLER, G., ZIMMER, I., SCOLARO, A., CAMPAGNA, C., PLÖTZ, J., BORNEMANN, H., TEILMANN, J. and MCMAHON, C. R. (2007). All at sea with animal tracks; methodological and analytical solutions for the resolution of movement. *Deep Sea Research Part II* **54** 193–210.
- ZIDEK, J. V., LE, N. D. and LIU, Z. (2012). Combining data and simulated data for space-time fields: Application to ozone. *Environ. Ecol. Stat.* **19** 37–56. [MR2909084](#)

Y. LIU
 J. V. ZIDEK
 DEPARTMENT OF STATISTICS
 UNIVERSITY OF BRITISH COLUMBIA
 3182 EARTH SCIENCES BUILDING
 2207 MAIN MALL
 VANCOUVER, BC V6T 1Z4
 CANADA
 E-MAIL: yang.liu@stat.ubc.ca
jim@stat.ubc.ca

A. W. TRITES
 B. C. BATTAILE
 MARINE MAMMAL RESEARCH UNIT
 INSTITUTE FOR THE OCEANS AND FISHERIES
 UNIVERSITY OF BRITISH COLUMBIA
 ROOM 247, AERL, 2202 MAIN MALL
 VANCOUVER, BC V6T 1Z4
 CANADA
 E-MAIL: a.trites@oceans.ubc.ca
b.battaile@oceans.ubc.ca